Icarus 233 (2014) 316–327

Contents lists available at ScienceDirect

Icarus

journal homepage: www.elsevier.com/locate/icarus

Water budgets of martian recurring slope lineae

Robert E. Grimm *, Keith P. Harrison, David E. Stillman

Southwest Research Institute, 1050 Walnut St. #300, Boulder, CO 80403, United States

ARTICLE INFO

Article history:
Received 6 May 2013
Revised 25 October 2013
Accepted 11 November 2013
Available online 19 November 2013

Keywords:
Mars, climate
Ices
Geological processes
Mars, surface

ABSTRACT

Flowing water, possibly brine, has been suggested to cause seasonally reappearing, incrementally growing, dark streaks on steep, warm slopes on Mars. We modeled these Recurring Slope Lineae (RSL) as isothermal water flows in thin surficial layers driven by gravity and capillary suction, with input from sources in the headwall and loss to evaporation. The principal observables are flow duration and length. At 40% porosity, we find that flow thicknesses reaching saturation can be just 50 mm or so and freshwater RSL seasonally require 2–10 m^3 of H_2O per m of source headwall. Modeled water budgets are larger for brines because they are active for a longer part of each day, but this could be partly offset by lower evaporation rates. Most of the discharged water is lost to evaporation even while RSL are actively lengthening. The derived water volumes, while small, exceed those that can be supplied by annual melting of near-surface ice (0.2–2 m^3/m for a 200-mm melt depth over 1–10 m height). RSL either tap a liquid reservoir startlingly close to the surface, or the actual water budget is several times smaller. The latter is possible if water never fully saturates RSL along their length. Instead, they would advance like raindrops on a window, as intermittent slugs of water that overrun prior parts of the flow at residual saturation. Annual recharge by vapor cold trapping might then be supplied from the atmosphere or subsurface.

1. Introduction

Repeat observations by the High Resolution Imaging Science Experiment (HiRISE) on the Mars Reconnaissance Orbiter revealed narrow (0.5–5 m), relatively dark streaks on steep slopes (25–40°) that appear and grow in warm seasons and fade in cold seasons (McEwen et al., 2011; Fig. 1). They appear mostly at southern mid-latitudes (32–48°S). Correlation of these Recurring Slope Lineae (RSL) with maximum surface temperatures >250 K led McEwen and colleagues to hypothesize that they were formed by flows of briny water, with the brine provided by subsurface seeps or hygroscopic salts. In a companion paper (Stillman et al., submitted for publication; hereafter Paper I), we demonstrate that southern mid-latitude RSL lengthening is generally limited to times when afternoon surface temperatures exceed 273 K: this allows the source to be fresh water or relatively pure ice. (Note that Paper I identifies the seasonal start of RSL flow as $L_s = 245° \pm 11°$, whereas 252° is used herein. This small discrepancy is due to new data that were incorporated into Paper I). McEwen et al. (2013) argue that equatorial RSL are also active for "peak" temperatures as low as 250 K. However, peak surface temperatures near the equator are reached earlier in the day than measured by orbital flyovers and so it cannot be ruled out that RSL are in fact active only >273 K. Whether fresh or briny, the inference that RSL are manifestations of contemporary flowing water is a breakthrough in Mars science observations.

In this paper, we assess the source volumes and longevity—the overall water budget—for martian RSL by modeling the interaction between input and evaporation in a shallow groundwater flow. We have previously used a multiphase H_2O and heat transport code to model the secular groundwater evolution of Mars (Grimm and Painter, 2009). However, this code is too slow to examine in detail the parameter space spanning hydraulic conductivity, evaporation rate, and the thickness, length, and duration of flow. Therefore we selected a simpler initial approach for the RSL problem, by explicitly modeling isothermal unsaturated groundwater flow and parameterizing the effects of phase changes and vapor transport. This allows us to develop scaling relationships for the principal factors controlling flow, facilitating extrapolation to conditions beyond a limited number of model runs. We demonstrate a point agreement between the approximate and "exact" codes. Finally, we interpret the model results in light of likely available H_2O volumes.

2. Conceptual model

The incremental growth of RSL—of order 1 m per sol—indicates they are not surface runoff, but subsurface flows. If these flows are not confined from below, vertical spreading would imply that the visible RSL represent such a small fraction of the discharge that the total water budget becomes unreasonable. Therefore we

* Corresponding author.
E-mail address: grimm@boulder.swri.edu (R.E. Grimm).

0019-1035/$ - see front matter © 2013 Elsevier Inc. All rights reserved.
http://dx.doi.org/10.1016/j.icarus.2013.11.013

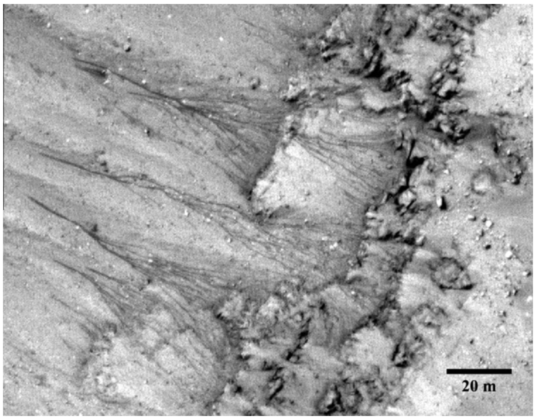

Fig. 1. RSL issuing from bedrock on the walls of an unnamed crater located on the west rim of the Hellas basin. North is up, flow is SE to NW. Note merging. HiRISE image PSP_005934_1400 acquired 1 November 07, $L_s = 340.5°$, center 39.6520°S, 88.1005°E.

envision RSL forming by flowing water in a thin surficial layer (Fig. 2). The underlying aquitard could be bedrock, but the only requirement is that its hydraulic permeability is significantly less than the unit in which flow takes place. For the sands and silty sands we consider for the surficial unit, terrestrial analogs for an incompletely consolidated aquitard also include sandy silt, silt, loess, and till (see tabulation in Freeze and Cherry, 1979). Alternatively, the aquitard could be created dynamically by freezing at the base of the flow front (Kreslavsky and Head, 2009). Special geological stratification is not required to propagate RSL in this case. Flows in the first several seasons after the RSL source is activated might experience large loss to the subsurface, but later recurrences would not. Melting temperatures reach depths of 40–650 mm in regolith depending on ice salinity and pore saturation (Table 1). Thus, thicknesses up to hundreds of mm are plausible for seasonal water flows on Mars. In Paper I, we attribute the widespread occurrence of nonheadwall-sourced RSL following the Mars Year 28 dust storm to melting of deeper, prior-RSL ground ice.

If RSL are formed by water, capillary suction must be an important force, in order to darken the surface by moistening along the length of the RSL. If capillary suction was negligible—say the material was coarse sand or larger, and the layer thick—then gravity would drive the unconfined flow into a parabolic longitudinal cross-section (Dupuit Equation), with the elevation of the water table varying from a maximum at the source to a minimum at the flow's nose: there would be no extended surface manifestation as RSL. The surface would be reached only with an input flux large enough to cause runoff, which we ruled out above based on the low apparent speed of RSL. We do know that capillarity does not completely dominate over gravity, because the flows largely move downhill instead of spreading in all directions. Secondary capillary suction through a fine-grained or poorly sorted surficial layer would wick water to the surface and cause surface darkening.

Evaporation and sublimation must play key roles, complementary to the source input, in the evolution of RSL. Such losses are the most plausible mechanisms for reversion of dark-toned RSL to the lighter background. However, Paper I shows that the period during which RSL are dark is divided into an early growth phase and a later stationary phase (see also Fig. 3). We propose two hypotheses for this observation. In the first hypothesis ("equilibrium flow"), RSL grow until balance is attained between input and the integral of evaporation along the length of the flow. RSL subsequently appear dark and stationary until the annual source is exhausted or frozen; then they fade as H_2O is lost without replenishment. Equilibrium flows must be briny, because surface temperatures during the stationary phase are <273 K (Paper I). In the second hypothesis ("slug flow"), RSL stop growing due to source cut-off but remain dark during the following stationary phase until the saturation falls below some threshold, perhaps where most capillary water is stripped. Under this latter hypothesis, RSL can be freshwater because they are stationary after afternoon surface temperatures have fallen below 273 K. Because evaporation is important in both of these conceptual flow models, the total water that has moved through RSL may exceed the volume inferred simply from the observed dimensions and assumed flow thickness.

Loss of H_2O from RSL to the atmosphere is important year-round. RSL frequently follow the same paths, presumably controlled by subtle topography. If the flow is indeed confined to a layer, evaporation and sublimation when RSL are faded (the "off-season") must completely remove subsurface H_2O to the annual flow depth, else repeated seasonal filling would eventually choke off the flow. Therefore a balance must exist such that regolith properties sufficiently restrict evaporation in spring and summer so that RSL can manifest, but allow enough loss in fall and winter to remove residual ice. Although loss rates are much smaller, the "off-season" duration is much longer than the "RSL season."

We have defined a conceptual model for RSL in which a source of readily available liquid discharges into a permeable layer and is acted upon by gravity, capillary suction, and evaporation, subject to the specific properties of the layer and constrained by the length and duration of RSL. We now elaborate on the numerical model and its parameters.

3. Numerical model

3.1. Method

We used the Variably Saturated Flow (VSF) process for MODFLOW (Thoms et al., 2006) to simulate RSL. The Richards

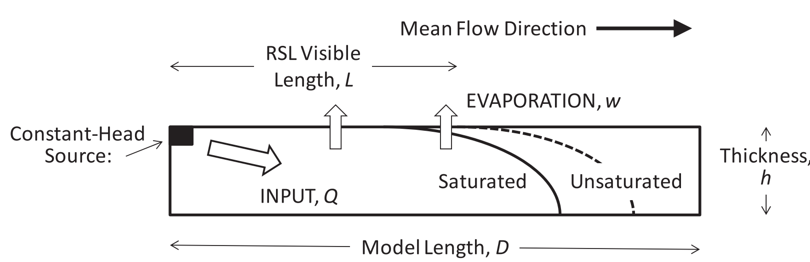

Fig. 2. Conceptual model for RSL: flow occurs in a thin layer and maximum length is determined by the balance between water input and water evaporated. Model is implemented as an isothermal two-dimensional flow in a domain of length *D* and thickness *h*. The model is actually sloped at 30° and is flattened in this drawing for compactness. The sides and bottom are impermeable: the last represents either bedrock or a saturated frozen sublayer. The source is a constant-head cell that allows variable input *Q*. Dashed line indicates partial saturation at which surface darkens, causing the visible RSL. Evaporation *w* acts across the top of the domain, for simplicity on the visible RSL only. Flow is driven by topographic gradient and by capillary suction calculated for the surficial analog material JSC-Mars-1. Note that capillary forces must wick water to and along the surface, else the flow front would exist almost entirely in the subsurface between the source and toe.

Table 1
Parameters for RSL variably saturated flow model and supporting calculations.

	Parameter	Min	Max	Ref. value	Notes
Reference thermal parameters					
1	Thermal conductivity, W m^{-1} K^{-1}	0.085	2.5	–	Dry (Zent et al., 2010) to saturated regolith
2	Specific heat capacity, J kg^{-1} K^{-1}	840	1525	–	See above
3	Bulk density, kg m^{-3}	1250	2000	–	See above
4	Freezing temperature, K	252	273	–	Pure water vs. NaCl eutectic
5	Max. annual melt depth, mm	40	650	–	See Fig. 5 for surface-temperature time series
Parameters for VSF model runs					
6	Flow thickness, mm	10	1000	–	Assigned based on range of Line 5
7	Hydraulic permeability at saturation, 10^{-12} m^2 (darcy)	0.2	6	–	1.93 darcy is logarithmic mean of measurements of JSC-Mars-1 by Sizemore and Mellon (2008)
8	Evaporation rate, mm/h	0.01	10	–	Sears and Chittenden (2005), Chevrier et al. (2007) and Bryson et al. (2008)
Parameters for extrapolation of model runs and derivation of water budgets					
9	Duration of RSL growth, sol	–	140	60	Fig. 2 and Stillman et al. (submitted for publication). Ref. value for non-merging RSL
10	RSL lifespan, sol	140	300	210	Growth + static phases. Stillman et al. (submitted for publication)
11	Minimum final flow length, m	–	–	50	McEwen et al. (2011), Stillman et al. (submitted for publication)
12	Flow thickness, mm	15	200	50	
13	Hydraulic permeability at saturation, darcy	1	100	–	Min = JSC-Mars-1, Max = upper limit for silty sand = median for clean sand (Freeze and Cherry, 1979)
14	Activation energy for H_2O loss, kJ/mol	51	67	60	Ingersoll (1970), Mellon et al. (2004), Sears and Chittenden (2005)
15	Minimum average loss rate for an active 50-mm flow, mm/h	0.06	0.08	–	Assumes loss rate $\propto$ vapor density $\propto \exp(-E_a/RT)/T$. Allows residual ice to sublimate in off-season
16	Fraction of diurnal cycle for flow activity	0.20	0.36	–	50-mm flow
17	RSL headwall fraction	~0.1	~0.9	0.5	Highly variable
18	Size of source zone, km	–	–	0.1	

Reference value is a best point-estimate.

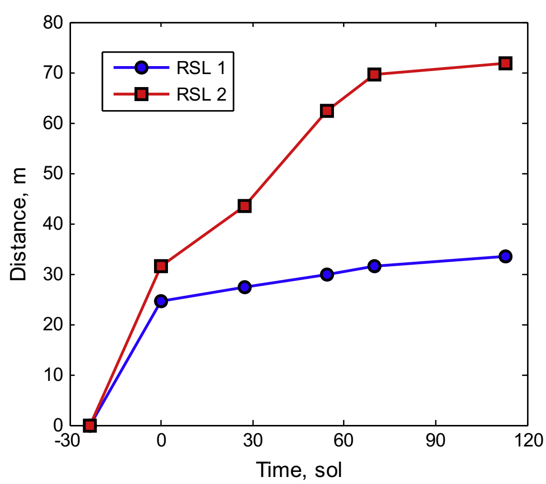

Fig. 3. Example of growth of individual RSL segments (Raga crater, 48.1184°S, 242.4470°E) that do not intersect or are not intersected by other RSL. Origin time was interpolated between HiRISE images ESP 020947 1315 (L_s = 217°) and ESP 02154 1315 (L_s = 245°). RSL 1 was already near maximum length when first imaged. Steady growth in RSL 2 was captured over several images. From these data, we infer a typical growth phase of ~60 sols for individual RSL: the overall growth phase of ~95 sols for an RSL region is due to merging.

Equation for flow in an incompressible 2D (z-vertical) porous medium with variable saturation is

$$\frac{\partial}{\partial x}\left[K_x(\psi)\frac{\partial H}{\partial x}\right]+\frac{\partial}{\partial z}\left[K_z(\psi)\frac{\partial H}{\partial z}\right]+W=C(\psi)\frac{\partial H}{\partial t} \quad (1)$$

where H is the hydraulic head (m), ψ is the pore-water pressure head ($\psi = H - z$), K_i is the hydraulic conductivity in the ith coordinate direction (ms^{-1}), W is the fractional change in storage per unit time due to sources and sinks (s^{-1}), and C is the specific moisture capacity (m^{-1}). Note that VSF includes matrix and fluid compressibility, but they have no effect on this problem and so are omitted. The flow is also assumed to be isothermal (freezing is later parameterized for the purpose of extrapolating the VSF results to an entire "flow season." Furthermore, Appendix A shows a test model for comparison that explicitly includes freezing and vapor transport). The hydraulic conductivity is assumed to be isotropic and is expanded as

$$K(\psi)=k_r(\psi)\frac{k\rho g}{\eta} \quad (2)$$

where k_r is the relative permeability (varies from 0 to 1 depending on pore-water pressure head; see below), k is the permeability at saturation (m^2), ρ and η are the density and dynamic viscosity, respectively, of water, and g is the gravitational acceleration (3.7 m/s^2). We take the logarithmic mean of permeability measurements of bulk JSC-Mars-1 by Sizemore and Mellon (2008) as a reference value $k_0 = 1.93 \times 10^{-12}$ m^2 (1.96 darcy) and express saturated hydraulic conductivity relative to the corresponding reference value, $K' = K/K_0$. The density and viscosity are fixed at 1100 kg/m^3 and 1.4×10^{-3} Pa s, respectively, intermediate between freshwater and NaCl eutectic brine (CRC, 2008). In this way the hydraulic conductivity of either endmember is within ~25% of the selected value. The exact fluid properties of either freshwater or brine have little impact on outcomes and the isothermal model applies equally to either. The principal effect of fluid composition in this paper (addressed later) is the longer daily duration of brine flow.

The porosity ϕ and effective or relative saturation S_e define the volumetric water content $\theta = \phi S_e$. The mean of bulk porosity measurements of JSC-Mars-1 is 0.64 (Sizemore and Mellon, 2008). This is an unusually large value, due to nonconnected vesicular porosity of the grains themselves and electrostatic "fairy castle" support in this Hawaiian tephra. Instead we assign $\phi = 0.4$, a typical value for sand. The right-hand side of Eq. (1) can be more intuitively understood as the change in saturation by noting that $C\,\partial H/\partial t = \phi\,\partial S_e/\partial t$. The specific moisture capacity is the slope of the volumetric soil–water characteristic curve, $C(\psi) = \partial\theta/\partial\psi$. In practice, the soil–water characteristic curve is expressed in terms of relative saturation, with the widely used parameterization of van Genuchten (1980):

$$S_e(\psi) = \frac{\theta - \theta_r}{\varphi - \theta_r} = \begin{cases} \frac{1}{\left[1+(|\alpha\psi|)^{n_v}\right]^{m_v}} & \psi < 0 \\ 1 & \psi \geqslant 0 \end{cases} \tag{3}$$

where θ_r is the volumetric residual saturation and n_v, m_v, and α are the van Genuchten parameters. VSF uses the Mualem model $m_v = 1 - 1/n_v$, so only n_v and α can be specified independently. Dinwiddie and Sizemore (2007) calculated $\psi(\theta)$ for JSC-Mars-1 from a physicoempirical model based on grain (pore) size distribution, and they fit these data with three free van Genuchten parameters. Our two-parameter fit yielded $\alpha = 1.7\ \mathrm{m}^{-1}$ and $n_v = 2.1$ (hence $m_v = 0.52$), with $\theta_r = 0.03$. These values are consistent with sands (Stephens, 1996).

The van Genuchten formula (3) can be rewritten as

$$C(S_e) = \frac{\partial\theta}{\partial\psi} = -\frac{n\,m_v\alpha(1 - S_r)}{1 - m_v} S_e^{1/m_v}\left(1 - S_e^{1/m_v}\right)^{m_v} \tag{4}$$

where $S_r = \theta_r/\theta_s$ and

$$k_r(S_e) = S_e^{1/2}\left[1 - \left(1 - S_e^{1/m_v}\right)^{m_v}\right]^2 \tag{5}$$

The soil–water characteristic curve Eq. (4) is used to calculate the pore water pressure head, which is added to the elevation head so that Eq. (1) can be solved for the flow.

Boundary conditions are no-flow on the sides and bottom of the model domain (Fig. 2), with input through a constant-head cell in the upper left and loss via evaporation across the top. The model has a constant thickness and is sloped at 30°. A constant-flux input might be more appropriate if RSL sources are volume- or rate-limited over the duration of seasonal flow: a constant-head condition is most appropriate for a reservoir that is large compared to the effluent. However, input fluxes are nearly constant over the runs, so each model can be matched to a specific input flux. If the flux were increased over the natural capacity, ponding or runoff would occur; if the flux were decreased, the flow would dry out from the rear. Neither is yet observed, so we conclude that the constant-head condition is acceptable, and it obviates introduction of additional parameters (repeat flows in a single season are treated qualitatively in the Section 6). It does not matter whether the input is at the top or bottom of the layer, because the flow length is much larger than the layer thickness. The size of the model domain is adjusted for different runs but flows are never allowed to reach the right-hand boundary. The initial head in all models was set at −10 m in order to produce near-residual initial saturations throughout.

VSF treats evaporation similarly to fluxes in all MODFLOW modules, as variants on Darcy's Law: flux is equal to the product of a conductance and a difference in pressure head. We adjusted the conductance as a function of capillary suction so that the evaporation rate was constant. We further restricted evaporation to surface points with $\theta > 0.17$, our assumed saturation at RSL darkening (see Appendix B). This simplified treatment neglects variable evaporation along the RSL and vapor flow in the subsurface. However, most of the volume evaporated would be from the saturated part of the RSL at the surface, which is where our approximation concentrates. The fractional volumetric loss rate W (s^{-1}) in the top row of saturated cells is equal to the evaporation rate w (ms^{-1}) divided by the cell height for unit cross-sectional width.

Constant evaporation rate is a specified parameter. Pure water will evaporate at ~1 mm/h at 273 K under an H_2O-dry, 7 mbar CO_2 atmosphere (Ingersoll, 1970; Sears and Chittenden, 2005). Salts can decrease the evaporation rate by a factor of ten if present at supereutectic concentrations (Altheide et al., 2009). Very low vapor pressures below freezing also lower evaporation rates, but this is irrelevant because Paper I demonstrates RSL flow occurs >273 K. Alternatively, fine-grained regolith tens of millimeters thick can produce an order-of-magnitude decrease in the sublimation rate of pure ice (Chevrier et al., 2007; Hudson et al., 2007; Bryson et al., 2008).

3.2. Results and analysis

Thirty-six VSF runs were carried out spanning layer thickness h = 10 mm to 1 m, saturated hydraulic conductivity K' = 0.2–6 relative to the reference value for JSC-Mars-1, and evaporation rate $w = 10^{-2}$ to 10 mm/h (Fig. 4). We measured the flow length L (m), the input water volume A per unit length of headwall (m^3/m), and the ratio Λ of water volume lost via evaporation to that retained in the flow at 30, 60, 120, and 240 sols. We independently determined the asymptotic (equilibrium) flow length L_{eq} and time t_{eq} when the flow reached 90% of its final length.

In order to interpret and generalize these results, we performed multiple regression using dimensionless quantities determined by the Buckingham Pi Theorem (e.g., Welty et al., 1984; Holsapple, 1993). The six variables (h, k, w, L, A, t) have only two fundamental dimensions (length and time), so four pi-groups can be formed. Selecting h and k as core variables, we find $\pi_1 = w/k$, $\pi_2 = L/h$, $\pi_3 = kt/h$, and $\pi_4 = A/h^2$. The dimensionless quantity Λ can be analyzed as another dependent variable. Power laws of the form $\pi_i = a\pi_j^b\pi_k^c\pi_l^d\ldots$ are then solved by least-squares inversion of $\mathbf{Gm} = \mathbf{d}$, where $\mathbf{d}$ is the column vector $\log(\pi_i)$, $\mathbf{m}$ is the column vector of coefficients $\log(a)$, b, c, $d\ldots$, and the rows of $\mathbf{G}$ are $[1, \log(\pi_j), \log(\pi_k), \log(\pi_l)\ldots]$. The a coefficients were empirically adjusted to better fit the thinner flows. Rounding the exponents to the nearest 0.1 and re-expanding to the original dimensional variables yields

$$A = 0.2K'^{0.9}w^{0.1}t\,h \tag{6}$$

$$\Lambda = 0.02\,w\,t^{1.1}K'^{0.1}/h^{1.1} \tag{7}$$

$$L_{eq} = 5K'h/w \tag{8}$$

$$t_{eq} = 40K'^{0.1}h/w^{1.1} \tag{9}$$

where the leading coefficients are rounded to one significant figure. K' is dimensionless; the other units are w = mm/h, t = sols, and h = meters. These fits are superposed on the original model results in Fig. 4.

We see the fundamental relationships more clearly by further rounding the exponents to zero or one, so that $A \propto Kth$, $\Lambda \propto wt/h$, $L_{eq} \propto Kh/w$, and $t_{eq} \propto h/w$. The water input increases linearly with time, showing the equivalence of constant-head and constant-flux boundary conditions. The ratio of evaporation rate to layer thickness controls the ratio of loss to storage and the equilibrium flow length and time: higher evaporation rates force the flow to reach equilibrium faster, resulting in a shorter final length. Higher hydraulic conductivity increases the total flux accommodated and the equilibrium length.

Eqs. (6)–(9) capture the essential behavior of RSL flow under isothermal conditions. We find reasonable agreement in a point comparison with a non-isothermal MarsFlo test case, detailed in Appendix A.

4. Water budget and recurrence longevity

Eqs. (6)–(9) can now be applied to the water budgets of RSL over one season given constraints on flow dimension and timing. Furthermore, the number of recurrences can be estimated given constraints on the source dimensions and age. Here the parametric adjustments for temporal variations in liquid content and vapor

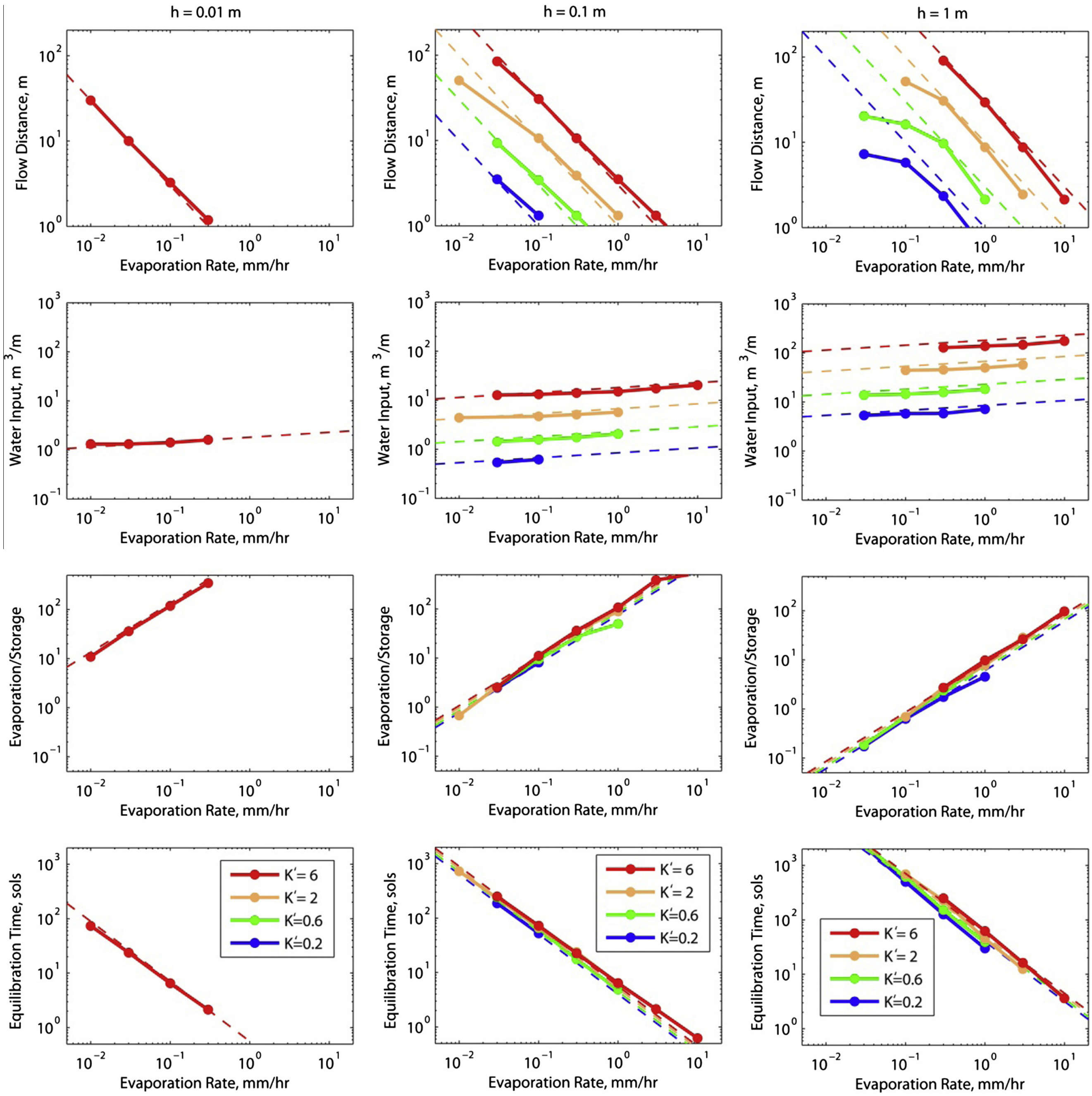

Fig. 4. Results of RSL unsaturated-flow models. Each column depicts a different value of the layer thickness h and colored curves vary the maximum (saturated) hydraulic conductivity K', normalized to JSC-Mars-1. Abcissa is the evaporation rate w. Symbols and solid lines indicate numerical models; dashed lines are multiple-regression fits, weighted toward the thinner layers. These fits include weak terms Eqs. (6)–(9) that are not included this caption summary. *First row*: Equilibrium flow length $L_{eq} \propto Kh/w$ (curvature indicates models that did not attain equilibrium). *Second row*: Total water input $A \propto Kht$. Plot is at 180 sols. *Third row*: Ratio of evaporation to storage $\Lambda \propto wt/h$ and is also plotted at 180 sols. $\Lambda > 1$ indicates more water has been lost to evaporation than remains in the visible RSL. *Fourth row*: Time until flow reaches equilibrium $t_{eq} \propto h/w$, numerically defined as when the flow achieves 90% of its asymptotic length. (For interpretation of the references to color in this figure legend, the reader is referred to the web version of this article.)

flux must be included, which require calculation of subsurface temperatures and scaling of loss rate.

4.1. Constraints

Four constraints are applied to the models. The first two restrict the allowable portion of the parameter space and the second two influence the water budget.

4.1.1. Flow length

RSL can be traced to hundred of meters but this is almost always after merging with other RSL. The zone of RSL advances in aggregate by repeated upstream merging (see Paper I). Fig. 3 shows two RSL that can be seen individually to grow and reach the stationary phase, for which the average length is ∼50 m. We take 50 m as representative of the minimum length RSL must achieve.

4.1.2. Flow duration and state

Under the assumption of equilibrium flow, we evaluate the regression equations at 210 sols (just under the mean time from the appearance of RSL to the beginning of fading), and we require $30 < t_{eq} < 120$ sols (the observed duration until growth ends). For slug flow, we evaluate the model at 60 sols (the mean time until growth ends) and require that the flow has *not* reached equilibrium in this time.

4.1.3. Time adjustment for freezing

We allow that one sol of flow is not one sol of calendar time due to diurnal freezing, so we calculate the fraction of time that flows are liquid and scale appropriately. Results are always expressed as calendar time. For the temperature model described below, this results in ~6 h per sol of freshwater flow. NaCl brines could be above the eutectic temperature for ~11 h per sol, but as an upper limit, we allow brine flows to be continuously active to encompass salts with very large freezing-point depression, e.g., $Mg(ClO_4)_2$. We assume a eutectic composition; therefore we do not treat decreasing liquid volume as the eutectic temperature is approached.

4.1.4. Minimum evaporation rate

We apply a minimum evaporation rate during RSL activity such that evaporation and sublimation in the off-season will empty the layer to depth *h*.

We now describe the temperature and loss models used to evaluate the last two constraints.

4.2. Surface temperature

Surface temperatures on Mars can be modeled principally from the insolation history and surface properties (e.g., Kieffer et al., 1977). RSL sites are geographically distributed and have a range of surface thermal inertias (McEwen et al., 2011; and Paper I); furthermore, temperatures must be evaluated throughout the year. It would be unnecessarily tedious to evaluate and average so many models for the purposes of this preliminary investigation. Instead, we fit a simple function to aggregate TES data around RSL at mid-southern latitudes that includes sinusoidal annual and diurnal variations and also annually modulates the amplitude of the diurnal signal:

$$T = 220 - 37\sin(\Theta) + [7\sin(\Theta) - 41]\sin(\Phi) \tag{10}$$

where $\Theta = 2\pi L_s/360$ and $\Phi = 2\pi L_s/0.538$ are the annual and mean diurnal time functions, respectively. This function does not reproduce the true non-sinusoidal diurnal variation due to thermal inertia nor changes in length-of-day vs. L_s. Mean phases are close to zero in the fit and so have been dropped; the fit does not acknowledge that TES measurements are not truly at diurnal extrema. Nonetheless, Eq. (10) is a good match to the overall annual and diurnal temperature variations (Fig. 5) and so can be used to roughly compute temperature (time) dependent loss rates and ground freezing. Ground temperatures are calculated analytically using the classical formula for periodic surface temperature (Turcotte and Schubert, 1982), with Eq. (10) converted to a 4-term Fourier series using the trigonometric identity for the product of sines. Material properties are elucidated in Table 1.

4.3. Annual H_2O loss and diurnal freezing

Because the unsaturated flow is isothermal in the VSF model, vapor diffusion and H_2O phase changes must be parameterized in this initial treatment. As described above, a constant evaporative loss rate *w* is specified. However, evaporation and sublimation must continue even when RSL are not active or have faded. Indeed, there must be a minimum loss rate set by the requirement that H_2O in the flow is removed completely in the "off-season" ($L_s = 314°$ or 16° back to 252°), else RSL would remain saturated with ice. Such loss must occur throughout the thickness of a regolith aquifer over bedrock; alternatively, the annual loss depth may

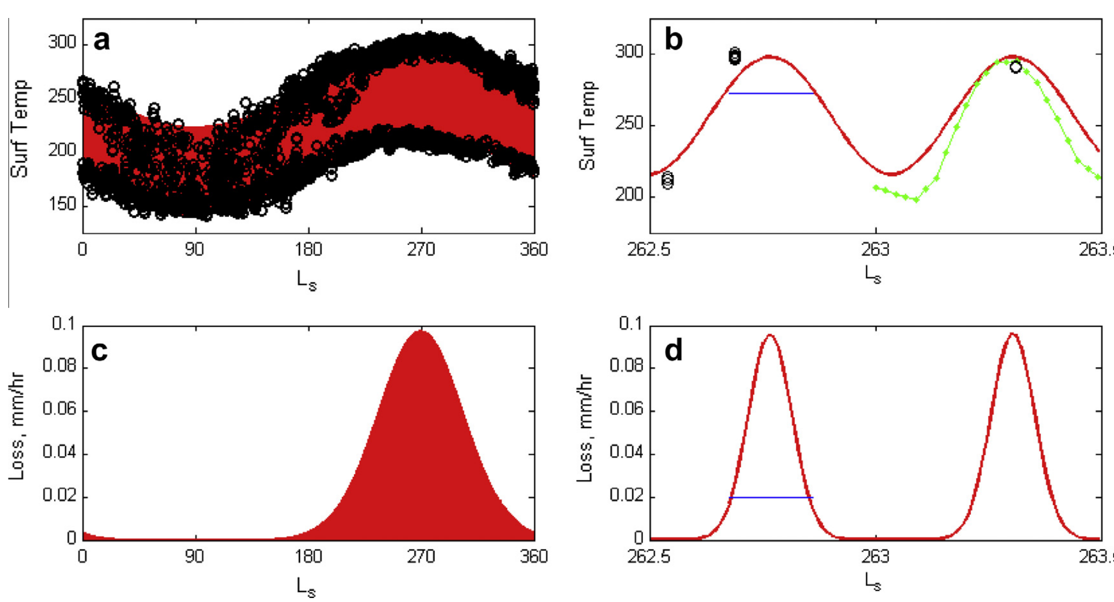

Fig. 5. (a) Surface temperatures at RSL sites recovered from PDS-archived TES data (symbols) and fit to four-term Fourier series (red). (b) Zoomed view near end of southern spring comparing diurnal cycles to Mars Climate Database surface temperature at 45°S 0°E (green, Forget et al., 2008). Phase mismatches occur because diurnal temperature cycle is not actually sinusoidal and our model considers only the mean martian sol. (c) Annual H_2O *minimum* loss curve and (d) diurnal zoom for a 50-mm thick layer. This model assumes that loss is proportional to the vapor number density computed at the surface using the temperature model above, and normalizes the sum in an RSL "off-season ($L_s = 314°$ or 16° for slug and equilibrium flow, respectively, to $L_s = 252°$) so that residual ice equal to the layer thickness is sublimated. Blue line in (b) is freshwater freezing temperature (273 K); corresponding line in (d) illustrates that almost all loss occurs when near-surface H_2O is liquid. (For interpretation of the references to colour in this figure legend, the reader is referred to the web version of this article.)

define the thickness of the aquifer over underlying residual ice (Kreslavsky and Head, 2009). Let wt be the total potential loss during RSL growth and possibly stationary phases, where w is understood to apply just to the "in-season" time- and depth-averaged loss rate, and t is the duration. Similarly, the "off-season" loss $w't' > h$, and $t + t' = Y$, one Mars year. In practice, we restrict t to only those times when water would be liquid at the surface (although the surface may be frozen most of the day even in summer, the loss will be dominated by the warmest times). If the fraction of the total loss occurring in-season is f, then $w > \frac{h}{t}\frac{f}{1-f}$. We can estimate f by assuming the H_2O flux is proportional to the vapor number density (Fick's Law). This is proportional to $e^{-E/RT}/T$, where E is an activation energy, T is temperature, and R is the gas constant. Theoretical and measured activation energies for sublimation and evaporation under Mars conditions vary from 51 to 67 kJ/mol (Ingersoll, 1970; Mellon et al., 2004; Sears and Chittenden, 2005): we adopt 60 kJ/mol. Other parameters are not required in this simple treatment because we are interested only in ratios of flux integrals. We find $f > 0.44$–0.69, so in turn w (mm/h) > (1.1–1.7)h (m). This range also accounts for the range in RSL timing under equilibrium or slug flow. An active (liquid) 50-mm flow therefore requires a minimum of ~0.07 mm/h evaporation such that 50 mm of ice can be sublimated during the period of inactivity.

4.4. Additional assumptions

Our two-dimensional model computes the source flux per unit length of headwall. If RSL do not occupy the entire lateral extent of the headwall, then the requirements on source volume are proportionately reduced. This fraction is highly variable: at the Horowitz crater type location, RSL appear nearly continuously along the headwall, whereas they are sparse in Fig. 1. We adopt 50% coverage as nominal.

The methodology developed above describes the water budget of RSL over one season. In order to extrapolate to the entire RSL source zone, an assumption must be made about either the number of seasonal recurrences N_R that a specified source dimension can support, or the size of a source that produces a fixed number of recurring flows. Without additional constraints, the choice is arbitrary as the scaling is linear. We assume RSL are drawn from a subsurface zone 100-m wide (perpendicular to the headwall) and 3-m thick, and calculate the number of recurrences allowed. The width is representative of ice-table recession in large pores (i.e., under binary diffusion) over 100 Kyr at 250 K (Eq. (30) in Painter, 2011). The thickness is representative of several meters of superficial icy mantle (Head et al., 2003) or 10 m or more of pore ice emplaced during a prior ice age (see Section 6). Atmospheric recharge of RSL is also treated in the Section 6.

5. Results

Figs. 6 and 7 contain the essential results of our analysis, for the assumptions of slug and equilibrium flow, respectively. We plot evaporation rate w vs. normalized hydraulic conductivity K' as in Fig. 4 and evaluate the water volume per length of headwall A, the ratio of evaporation to storage Λ, and the number of recurrences N_R subject to the constraints above.

For slug flow, the constraints on minimum length, minimum evaporation rate, and minimum equilibrium time jointly restrict the allowable parameter space (Fig. 6). For very thin flows (h = 15 mm), the freshwater input can be <1 m^3/m, which allows the nominal source zone to support up to 1000 seasonal recurrences. However, this must be accompanied by extraordinarily low loss rates, <0.1 mm/h. Such slow evaporation of freshwater would require screening overburden exceeding the flow thickness (Bryson et al., 2008). On the other hand, relatively thick flows (h = 200 mm) consume several tens of m^3/m water, so that the nominal source zone supports only a few dozen annual recurrences. Evaporation removes a smaller fraction of the effluent due to the large thickness and therefore rates approaching 1 mm/h can be sustained. The optimal flow thickness appears to be several tens of mm, in which seasonal water budgets allow hundreds of annual recurrences and evaporation rates are consistent with a fine-grained or poorly sorted overburden. At h = 50 mm, for example, the model calls for w = ~0.1 mm/h, A = 2–10 m^3/m, $\Lambda \sim 2$, and N_R = 100–300. One general result from all flow thicknesses is that hydraulic conductivity much higher than the JSC-Mars-1 reference is required, $K' > 10$.

The results for briny slug flows are similar to Fig. 6 and are not plotted. The acceptable region is reduced on the right-hand side, coincidentally, close to the minimum evaporation rate. Lower evaporation rates can be sustained in supereutectic brines without the need for screening overburden, but the lower bound due to off-season loss must still apply. Overall, the contours in each of the first two columns are a factor of ~3 higher than freshwater flow and the third column a factor of 3 smaller. Both of these effects are due to the longer daily duration of brine flow: the acceptable region contracts because equilibrium is reached faster and the total volume and loss/storage are just slightly smaller than the time multiplier of ~4. Recall, however, that brines were permitted to be continuously active, so these results are upper limits. The actual increase <2 in NaCl-brine duration would result in a proportionately smaller change in water volume.

For equilibrium flow, constraints imposed by the minimum flow length and both the minimum and maximum time to equilibrium considerably reduce the acceptable part of the parameter space (Fig. 7; note that boundaries do not abut between slug and equilibrium models due to differences in the assumptions about the duration of lengthening). For freshwater, these constraints are so tight that the minimum seasonal loss rate to enforce annual sublimation has no effect. At h = 50 mm, the seasonal water budget is >10 m^3/m, with $\Lambda > 10$ indicating >90% is lost to evaporation. This huge loss is due to the time that the flow remains stationary and at equilibrium, when all additional water is balanced by evaporation. The nominal source zone supports <30 annual flow recurrences. Evaporation rates can be a few times higher than for slug flows, however. Recall that freshwater is not favored for the equilibrium model because Paper I demonstrates the stationary phase is <273 K.

Brine flows reaching equilibrium (Fig. 7) are strongly displaced toward smaller evaporation rates because they spend so much time at full length losing many times their ground volumes. Although lower hydraulic conductivities area allowed, volume requirements are the largest of any model, 30–100 m^3/m for a 50-mm flow (note the minimum-evaporation constraint). A consequence is that the nominal source zone may sustain only a few dozen RSL recurrences.

6. Discussion

Our modeling best explains the length and seasonal duration of RSL as transient ("slug") near-surface flows of water perhaps 50-mm thick. This is consistent with a modest seasonal water flux (2–10 m^3/m). Evaporation rates during RSL activity (~0.1 mm/h are comparable to laboratory experiments of distilled H_2O under 10–40 mm of fine-grained material (Hudson et al., 2007; Bryson et al., 2008) or unobstructed loss from supereutectic brine (Altheide et al., 2009).

We did find that the saturated hydraulic conductivity must be greater than anticipated. The Mars-adjusted, normalized hydraulic

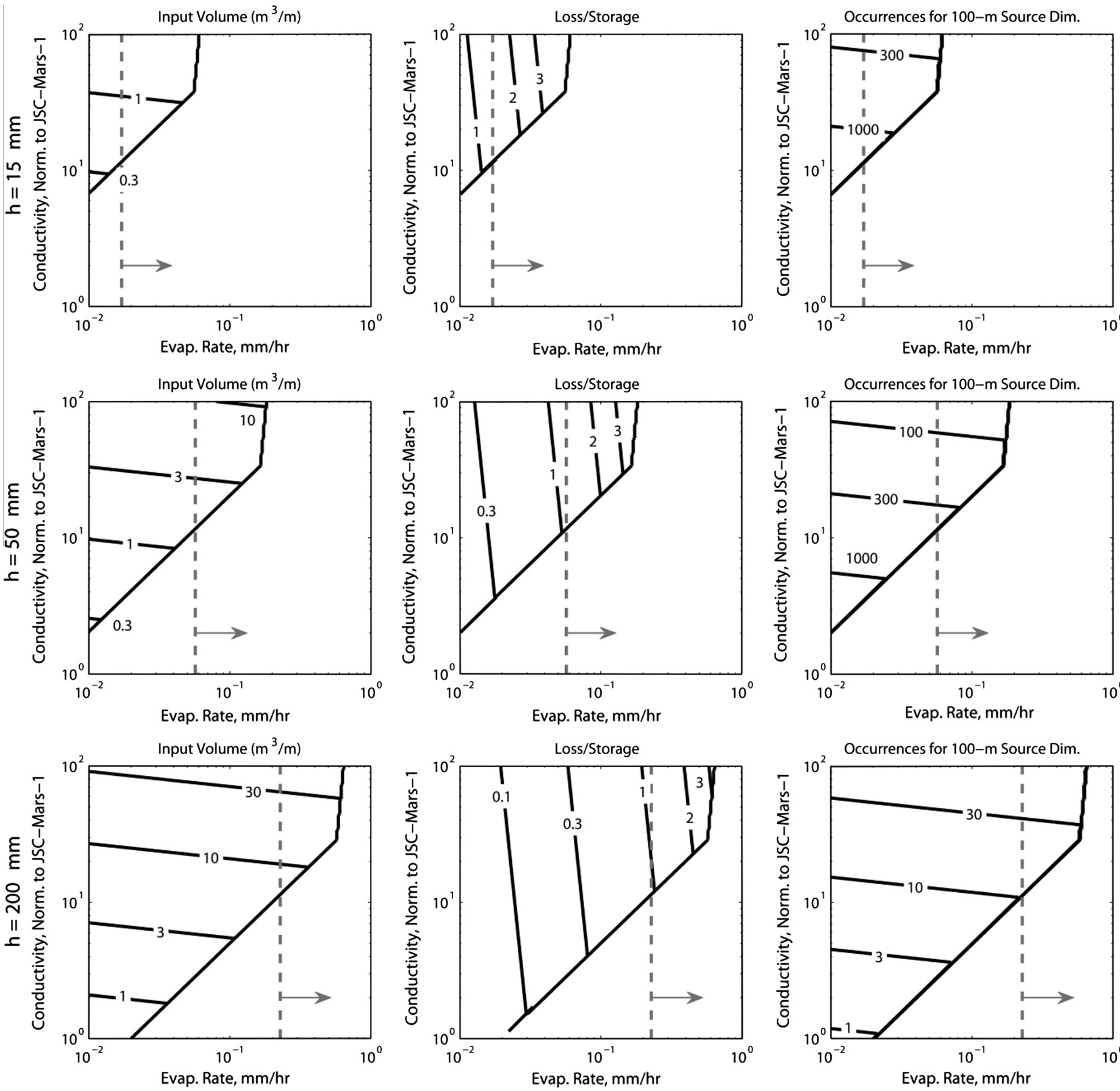

Fig. 6. Conditions for RSL freshwater slug flow extrapolated from numerical models using multiple regression. Lower-right cutoff is 50-m minimum length and upper-right cutoff eliminates models that reach equilibrium before 60-sol flow duration. Dashed gray line indicates minimum loss rate such that thickness > *h* of ice will sublimate during "off-season" (see text and Fig. 5). Flows 50-mm thick require several m^3/m of water annually and evaporative loss exceeds the water remaining in the RSL. Flows can recur hundreds of times for each 100-m width of an assumed equivalent 3-m thick H_2O source. Hydraulic conductivity must be 10–100 times that inferred for JSC Mars-1, corresponding to a clean sand. A thin covering of fine-grained or poorly-sorted material is likely necessary to restrict evaporation rates to ~0.1 mm/h. Brine flows (not shown) have right-hand cutoff close to minimum evaporation line and consume about three times as much water because they are active over a larger portion of the day. Minimum loss must still be enforced even if supereutectic brines have lower evaporation rate.

conductivity $K' = 10–100$ corresponds to permeability approximately 10–100 darcy. This lies at the upper end of permeability for silty sand or in the middle of the range for clean sand (Freeze and Cherry, 1979). JSC-Mars-1 can be described as a silty sand and so the derived permeability is within the range of such materials. However, the median grain diameter for JSC-Mars-1 is 250 μm, a medium-to-fine sand. Therefore JSC-Mars-1 without its unusual ultrafine fraction may be a good analog for the slope materials in which RSL form. We did not adjust the soil–water characteristic curve commensurately with the saturated conductivity. This is unlikely to strongly affect the results, because even coarse sand (mm-sized grains) would have capillary rise >100 mm on Mars and hence be able to wet the favored layer thicknesses.

Levy (2012) first brought hydrogeological arguments to bear on RSL. He recognized that incremental growth was related to groundwater. Levy assumed Darcy saturated flow and used the length, time, and assumed porosity to derive permeabilities in the 1 darcy range. This is an order of magnitude or more below our estimates because (1) the flow efficiency was overestimated: suction must

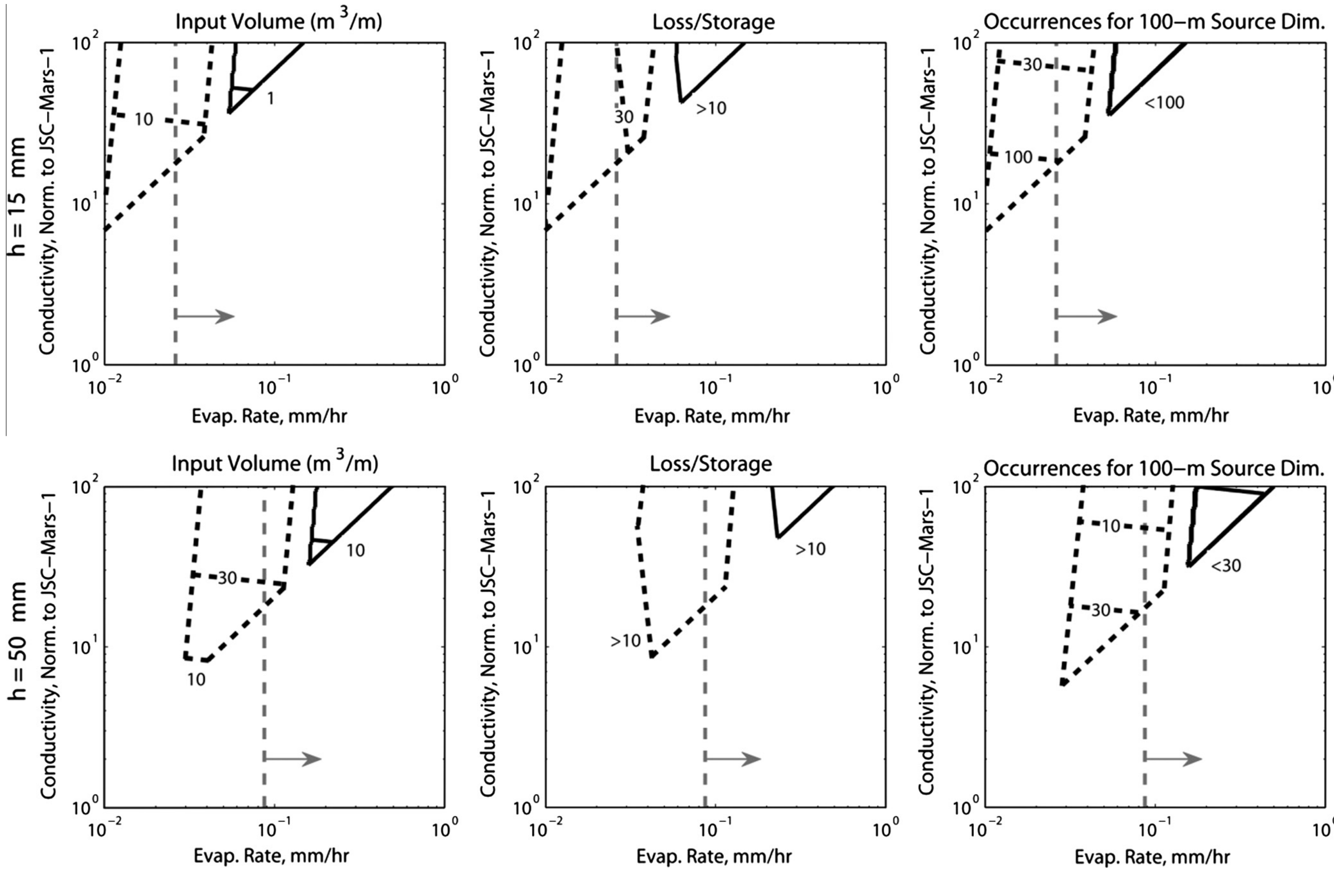

Fig. 7. Conditions for RSL freshwater (solid) and brine (dashed) equilibrium flow. Time to reach equilibrium is >120 sols and <60 sols at left- and right-hand cutoffs, respectively. Flow length is less than 50 m at the lower-right cutoff. Flow is carried out to a total duration of 210 sols. Acceptable freshwater model space is small and requires very large hydraulic conductivity. Due to the long times spent at equilibrium at maximum length, with incoming water evaporated along the length of the flow, water volumes and loss/storage ratios are large. Flows can then recur only dozens of times for the source zone described for Fig. 6. Brine flows again require more water and are largely constrained by minimum evaporation rate to enforce off-season loss.

fully wet an initially unsaturated medium before flow can advance at the Darcy pore velocity, and (2) the available time was overestimated by not accounting for the difference between growth and stationary phases.

Our observation in Paper I that southern mid-latitude RSL advance only when surface temperatures are >273 K supports the hypothesis that these flows are comprised of fresh water. Our "best-fit" flow depths of 50–100 mm (silty overburden plus sandy aquifer) lie within the ~150–200 mm depth at which diurnal temperatures in freshwater-saturated regolith reach the melting temperature. In contrast, Chevrier and Rivera-Valentin (2012) assumed that 100–200 mm of dry regolith overlie saturated regolith, which does not allow the 273 K isotherm to penetrate more than ~50 mm. This in turn led them to propose $CaCl_2$ or $Mg(ClO_4)_2$ eutectic brines as the only plausible liquids at 200-mm depth. We argued above that some water must be present at the surface, else the RSL would not appear dark, and so the thermal diffusivity within RSL must be higher. However, we acknowledge that RSL must propagate through material that probably has much lower thermal diffusivity than that of H_2O-saturated regolith. Our initial non-isothermal models (Appendix A) show that water can fill dry regolith quickly, providing a thermal conduit to diffuse subsequent temperature variations to depth. Nonetheless, our results show that even salts producing large freezing-point depressions do not change the inferred water volumes by more than a factor of three.

Our minimum modeled annual RSL water budgets of a few m^3 per meter of headwall are higher than that which can be derived by melting of surficial ice: 2 m^3/m of H_2O extruding over 5 m vertically translates to 1-m depth into the RSL headwall at porosity 40%, whereas the annual maximum depth of melting is a few hundred millimeters at most (Table 1). Either RSL draw on liquid reservoirs in communication with the annual melting depth, or the water budgets are somewhat smaller than predicted here.

An aquifer source for RSL remains thermodynamically challenging. Mellon and Phillips (2001) suggested martian "gullies" were sourced from aquifers, but they invoked fracturing to bridge the 100–200 m gap between the freezing isotherm and the colder surface. Because gas diffusion is slow, however, an ice- or water-bearing subsurface is probably always at or near the saturated vapor pressure, and so the depth to melting will depend almost exclusively on temperature. This allows liquid water to be closer to the surface than considered by Mellon and Phillips (2001): using their adopted heat flow (30 mW/m^2), thermal conductivity for fine-grained overburden (4.5×10^{-2} W/m K), and a surface temperature of 220 K, the average depth to the NaCl eutectic temperature could be as shallow as 50 m. This barrier is still too thick to be breached by the surface thermal wave even in a high-conductivity rock layer.

If RSL sources are restricted to lie within the annual melting depth, the water budgets are likely in the range 0.2–2 m^3/m (200-mm depth into the headwall over 1–10 m height), a factor of 5–10 smaller than estimated from the models developed here. This would be consistent with ~5% porosity instead of the adopted 40%. Although this is too small for the high-permeability sands required by the observed rates of RSL movement, it is typical of sand residual saturations. If the average water content of RSL was never far from residual saturation, RSL could be sourced entirely in the annual melt layer. We can then pose a new conceptual model for RSL flow as a series of discontinuous slugs instead of the continuous extrusion modeled here. When the source is intermittently cut off, the slug spreads out to residual saturation. Subsequent slugs overrun the earlier zone at residual saturation and spread out at the terminus, extending the RSL. This process is partly analogous to vertical infiltration of rainfall but is perhaps better pictured as raindrops on a window: each raindrop follows the path of earlier flow and then extends the water trace. The number, saturation, and duration of slugs introduce free parameters beyond the scope of this initial study, but can be modeled using both VSF and MarsFlo. Potential drawbacks to this model include higher hydraulic conductivity to allow the last slugs to reach the flow front and greater susceptibility to evaporation.

Annual cold trapping of vapor to provide even 200 mm of H_2O is problematic. Temperatures approaching 260 K are required to refill the melt layer from ice previously cold-trapped just below (40% porosity, 600 Pa CO_2, and neglecting the influence of pore size; see Mellon and Jakosky, 1993; Painter, 2011). If the very shallow subsurface was this warm, an aquifer could lie just beyond, obviating the need for vapor diffusion. On the other hand, external recharge would require just $2 \times 10^4\ m^2$ of atmosphere annually precipitating a full 10 μm of H_2O for each square meter of RSL headwall, but we pose no mechanism to localize precipitation. The diffusion problem remains, now reversed to top down. Melting and infiltration of early frost would significantly speed up the recharge.

Deliquescence has no advantages to water sourcing for RSL but significant drawbacks. Because the H_2O and salt masses are comparable in a hygroscopic salt hydrate, $\sim$1 m^3/m of water per season requires a comparable volume of salt that is able to bond to the water. Significant mass wasting would therefore accompany deliquescence, which is not observed (Kite, 2013). If the salt is somehow not transported away, new water must be provided for the next cycle, and the presence of salt is irrelevant to the H_2O transport except for possibly providing a freezing-point depression.

New kinds and cadences of observations may be necessary to better constrain RSL flow and source mechanisms. Perhaps the most straightforward would be a spacecraft with 45° orbital inclination that would view RSL at higher frequency than from polar orbits (Paige et al., 2012). Critical observations of seasonal growth phases, possible repeat flows along the same paths, and diurnal changes could then be made accurately. The large evaporative losses predicted here may be detectable from orbit or the ground.

7. Conclusion

We modeled martian recurring slope lineae as isothermal, groundwater flows in a porous medium, driven by gravity and capillary suction and subject to evaporation. We parameterized freezing and vapor transport. We applied constraints on RSL length and longevity derived in our companion paper. We found that annual water budgets can be as small as a few cubic meters per meter of headwall. Evaporation rates are bounded: the minimum is determined by the requirement that the residual ice must evaporate or sublimate during the majority of the year in which RSL are not visible, and the maximum is set by the requirement that the flow not come to equilibrium between input and loss. The derived evaporation rates $\sim$0.1 mm/h call for a shielding layer of 10–40 mm of fine-grained or poorly-sorted material over freshwater flows. Supereutectic brines might require little or no shielding. We found that flow thicknesses of 50–100 mm were optimal.

Our principal conclusion is that recurring slope lineae can be explained by relatively small quantities of liquid water, but the water budget nonetheless exceeds that which can be stored in the annually melted depth. Either RSL tap extraordinarily shallow aquifers, or the true water budget is smaller. The latter is plausibly the result of repeated small batches of water that follow the same path.

Acknowledgments

This work was supported by the NASA Mars Fundamental Research Program, Grants NNX12AH99G (R.E.G., K.P.H.) and NNX12AH95G (D.E.S.) We thank Tim Michaels for providing the TES-derived surface temperatures, Vicky Hamilton and Scot Rafkin for helpful discussions, and Mikhail Kreslavsky, Hanna Sizemore, and Alfred McEwen for constructive reviews. Comments by Colin Dundas on Paper I also strongly influenced this paper.

Appendix A. Proof-of-concept multiphase model with liquid and gas transport

We developed a numerical model for RSL that eliminates the parameterizations adopted in the text for H_2O phase transformations and gas diffusion. We used MarsFlo, which treats the behavior of solid, liquid, and gaseous phases of water in a partially saturated porous medium (Grimm and Painter, 2009; Painter, 2011). A carbon dioxide atmosphere occupies the unsaturated fraction of the pore space. Liquid flow is driven by pressure differences in saturated parts of the aquifer (Darcy flow) and by capillary pressure, while water vapor flow is driven by pressure gradients and the advection of the carbon dioxide component. The code has been successfully tested against analytically tractable problems and laboratory experiments (Painter, 2011). The purpose of this test was to demonstrate the feasibility of shallow freshwater flows in the presence of diurnal freezing and to make a point comparison to VSF.

A.1. Model description

The model domain is 1.9 m long, 1.4 m deep, and is stratified. The uppermost 10 mm has 10-μm grain size, appropriate to silt. The rest of the model has grain diameter 200 μm, corresponding to a fine-grained sand. The uppermost 60 mm begin saturated with 5 mbar of dry CO_2 vapor imposed from the overlying atmosphere. The entire model below 60 mm is initially saturated with H_2O ice. This state is intended to represent RSL regions just before the beginning of annual flow, where the prior year's flow has sublimated to some depth.

For the environment appropriate to the current study, vapor diffusion and liquid flow depend, respectively, on pore radius and permeability. These two parameters are in turn related to grain size. We use the approach of Costa (2006) to derive the effective pore radius and permeability of a cubic lattice arrangement of spherical grains. We derive a saturated permeability of $1.47 \times 10^{-11}\ m^2$ for the sand, i.e., about 8 times larger than that measured for bulk JSC-Mars-1 (Sizemore and Mellon, 2008). We modified MarsFlo to use the binary and Knudsen vapor diffusion coefficients of Mellon and Jakosky (1993) in their seminal study of ground ice stability on Mars. Typical binary diffusion coefficients are on the order of $10^{-3}\ m^2\ s^{-1}$, while Knudsen diffusion coefficients range from about 4×10^{-4} to $10^{-2}\ m^2\ s^{-1}$ over grain diameters of 10–200 μm.

A saturation-dependent mixing model (Painter, 2011) is used for thermal conductivity (the characteristics of pore and grain connectivity are not considered). The thermal conductivity of ice is weakly temperature dependent, averaging 2.7 W/m K over the range 200–273 K. Thermal conductivities of liquid water and carbon dioxide are fixed at 0.561 and 0.0146 W m^{-1} K^{-1}, respectively. The bulk thermal conductivity of the dry porous medium is 0.13 W m^{-1} K^{-1}.

The model domain is actually sloped at 30°. As with the VSF model, a constant-head boundary condition is applied to the upper end of the aquifer, allowing water to be drawn into the model as needed. Evaporation is not a parameterized boundary condition, but arises naturally from the modeled temperature-dependent vapor diffusion, and is free to vary with time. The right and lower model boundaries are no-flow. The temperature of the ground surface is varied according to Eq. (10) appropriate for observed RSL initiation at L_s = 245°.

A.2. Results

As melting temperatures are reached on the morning of the first martian day (Fig. A1) liquid water enters the model from the source region and flows downslope over the ice bed, preceded by a plume of vapor. In the afternoon, temperatures fall below freezing and an ice layer forms near the surface. The ice steadily thickens downward, eventually filling the layer.

The next morning, most of the previous day's flow is remelted. Melting can occur because the vapor pressure in the subsurface is above the triple point and cannot quickly diffuse to equilibrium with the 5-mbar atmosphere, but it should be noted that the overnight loss of latent heat does inhibit subsequent remelting. This is a key aspect of the physics that was not captured by simple calculations in the body of this paper and by others just using the depth to the melting isotherm.

The liquid does not advance significantly on the second day, however, suggesting it has already reached equilibrium within one sol of initiation and at a length approaching 1 m. The mean evaporation rate during active flow (Fig. A2) is 1.7 mm/h. This is much larger than permitted in the main text to achieve RSL slug flow to >50 m over 60 sols and it is close to the free evaporation rate (Sears and Chittenden, 2005). It is clear that the overburden is providing little shielding in this test case in which the large pores and loss rates were chosen to allow the model to converge readily.

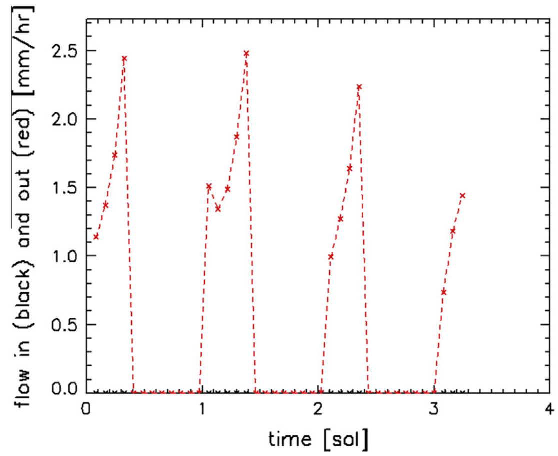

Fig. A2. Flux across the top boundary of the MarsFlo example in the previous figure. The very high loss (averaging 1.7 mm/h when the flow is active) in this example brings the flow to equilibrium in only about one sol.

Eqs. (8) and (9) above predict L_{eq} = 1.3 m and t_{eq} = 1.7 sols; we do not correct the time for overnight freezing because the MarsFlo equilibrium was apparently reached during the initial flow. We consider this reasonable agreement and conclude that Marsflo and VSF concur and that this exercise confirms the conceptual model of a diurnal cycle of melting, flow, and freezing.

Appendix B. Soil darkening experiments

We conducted soil darkening experiments with two soil samples: JSC Mars-1 (110 cm^2/g; Pommerol et al., 2009) and a sample fabricated from a mixture of sand and clay (Stillman and Grimm, 2011). The latter was selected to match the specific surface area inferred from Viking surface measurements (17 cm^2/g; Ballou et al., 1978). We photographed each soil sample with a digital SLR camera, for a range of moisture contents. Camera settings were fixed throughout the experiment, as was the light source. The phase angle was approximately 35°. Each image was stretched so that minimum and maximum values corresponded to fixed dark and light

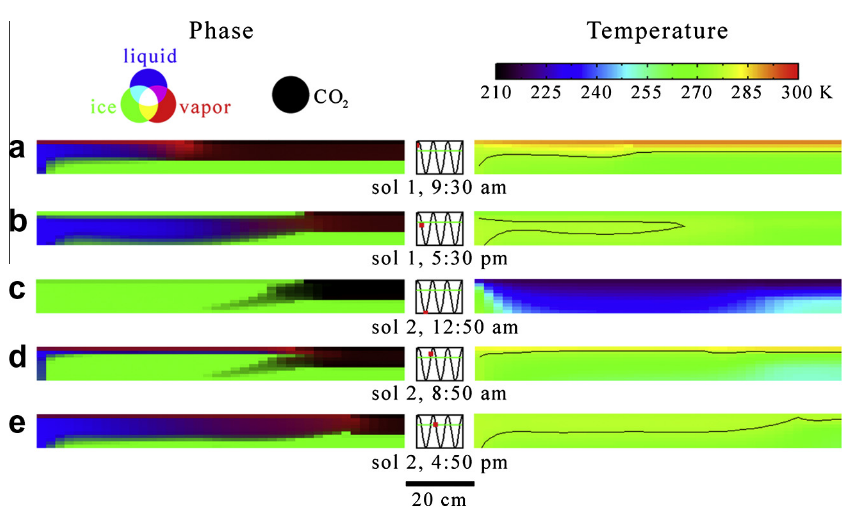

Fig. A1. Distribution of H_2O phases (left) and temperatures (right) in a MarsFlo proof-of-concept model of an RSL. Multiple H_2O phases in a single model cell are indicated by the color mixing scale (top left). The 30° slope downhill from left to right has been removed for more efficient display and there is no vertical exaggeration. Sublimation of frozen RSL from the previous year sets the initial ice-table depth at 6 cm. See text for other boundary conditions. Black lines in the temperature plots and green lines in the small center plots correspond to pure ice melting at 273 K. On the morning of the first sol of RSL flow, a plume of liquid and vapor flows downslope (a). As evening approaches, a shallow subsurface ice layer develops (b) and eventually engulfs the entire "aquifer" (c). As surface temperatures rise the following morning, melting allows the flow to resume (d and e). (For interpretation of the references to colour in this figure legend, the reader is referred to the web version of this article.)

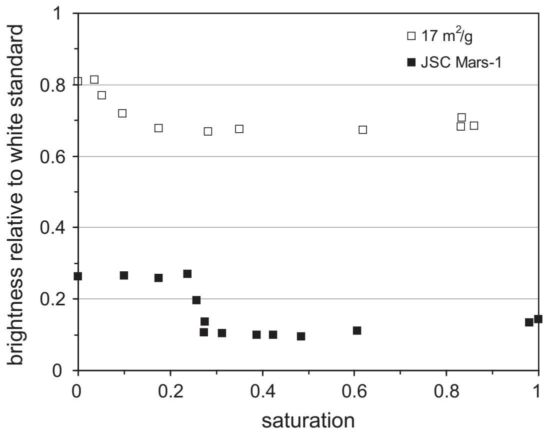

Fig. B1. Soil darkening as a function of water content under ambient laboratory conditions. JSC-Mars-1 has a very high specific surface area (110 m^2/g, Pommerol et al., 2009) and therefore adsorbs a relatively large amount of water before darkening. Sand–clay mixture matched to Viking soil (17 m^2/g: Ballou et al., 1978) requires relatively little water to darken. We used 17% saturation at darkening, the mean value of the transitions for the two materials.

test areas present in every image. The mean brightness of soil sample pixels was then computed (excluding any saturated pixels; Fig. B1).

References

Altheide, T., Chevrier, V., Nicholson, C., Densen, J., 2009. Experimental investigation of the stability and evaporation of sulfate and chloride brines on Mars. Earth Planet. Sci. Lett. 282, 69–78.

Ballou, E.V., Wood, P.C., Wydeven, T., Lehwalt, M.E., Mack, R.E., 1978. Chemical interpretation of Viking lander 1 life detection experiment. Nature 271, 644–645.

Bryson, K.L., Chevrier, V., Sears, D.W.G., Ulrich, R., 2008. Stability of ice on Mars and the water vapor diurnal cycle: Experimental study of the sublimation of ice through a fine-grained basaltic regolith. Icarus 196, 446–458.

Chevrier, V., Rivera-Valentin, E.G., 2012. Formation of recurring slope lineae by liquid brines on present-day Mars. Geophys. Res. Lett. 39. http://dx.doi.org/10.1029/2012GL054119.

Chevrier, V. et al., 2007. Sublimation rate of ice under simulated Mars conditions and the effect of layers of mock regolith JSC Mars-1. Geophys. Res. Lett. 34. http://dx.doi.org/10.1029/2006GL028401.

Costa, A., 2006. Permeability–porosity relationship: A reexamination of the Kozeny–Carman equation based on a fractal pore-space geometry assumption. Geophys. Res. Lett. 33. http://dx.doi.org/10.1029/2005GL025134.

CRC, 2008. Handbook of Chemistry and Physics, 88th ed. CRC Press, Boca Raton.

Dinwiddie, C.L., Sizemore, H.G., 2007. JSC Mars-1 soil moisture characteristic and soil freezing characteristic curves for modeling bulk vapor flow and soil freezing. Lunar Planet. Sci. 39, 2394.

Forget, F., Millour, E., Lewis, S.R., 2008. Mars Climate Database v4.3 User Manual. <www-mars.lmd.jussieu.fr>.

Freeze, R.A., Cherry, J.A., 1979. Groundwater. Prentice-Hall, Englewood Cliffs, 604pp.

Grimm, R.E., Painter, S.L., 2009. On the secular evolution of groundwater on Mars. Geophys. Res. Lett. 36. http://dx.doi.org/10.1029/2009GL041018.

Head, J.W., Mustard, J.F., Kreslavsky, M.A., Millikan, R.E., Marchant, D.R., 2003. Recent ice ages on Mars. Nature 426, 797–802.

Holsapple, K.A., 1993. The scaling of impact processes in planetary sciences. Annu. Rev. Earth Planet. Sci. 21, 333–373.

Hudson, T.L., Aharonson, O., Schorghofer, N., Farmer, C.B., Hecht, M.H., Bridges, N.T., 2007. Water vapor diffusion in Mars subsurface environments. J. Geophys. Res. 112. http://dx.doi.org/10.1029/2006JE002815.

Ingersoll, A.P., 1970. Mars: Occurrence of liquid water. Science 168, 972–973.

Kieffer, H.H. et al., 1977. Thermal and albedo mapping of Mars during the Viking primary mission. J. Geophys. Res. 82, 4249–4291.

Kite, E.S., 2013. Mass balance constraints on the sustainability of Mars' recurrent slope lineae (RSL): Should astrobiology be a priority? Present-Day Habitability of Mars, planets.ucla.edu/wp-content/form-data/mars-abstracts-2013/74-Kite_Habitability_2013.pdf.

Kreslavsky, M.A., Head, J.W., 2009. Slope streaks on Mars: A new "wet" mechanism. Icarus 201, 517–527.

Levy, J.S., 2012. Hydrological characteristics of recurrent slope lineae on Mars: Evidence for liquid flow through regolith and comparisons with Antarctic terrestrial analogs. Icarus 219, 1–4.

McEwen, A. et al., 2011. Seasonal flows on warm martian slopes. Science 333, 740–743.

McEwen, A. et al., 2013. Recurring slope linear in equatorial regions of Mars. Nature Geosci. http://dx.doi.org/10.1038/NGEO2014.

Mellon, M.T., Jakosky, B.M., 1993. Geographic variations in the thermal and diffusive stability of ground ice on Mars. J. Geophys. Res. 98, 3345–3364.

Mellon, M.T., Phillips, R.J., 2001. Recent gullies on Mars and the source of liquid water. J. Geophys. Res. 106, 23165–23179.

Mellon, M.T., Feldman, W.C., Prettyman, T.H., 2004. The presence and stability of ground ice in the southern hemisphere of Mars. Icarus 169, 324–340.

Paige, D.A. et al., 2012. Orbiting observatory for studying hydrologically active regions on Mars, concepts approaches Mars. Explor. Lunar Planet. Sci., #4235.

Painter, S.L., 2011. Three-phase numerical model of water migration in partially frozen geological media: Model formulation, validation, and applications. Comput. Geosci. 15, 69–85.

Pommerol, A., Schmitt, B., Beck, P., Brissaud, O., 2009. Water sorption on martian regolith analogs: Thermodynamics and near-infrared reflectance spectroscopy. Icarus 204, 114–136.

Sears, D.W.G., Chittenden, J.D., 2005. On laboratory simulation and temperature dependence of the evaporation rate of brine on Mars. Geophys. Res. Lett. 32, 2005G. http://dx.doi.org/10.1029/L024154.

Sizemore, H.G., Mellon, M.T., 2008. Laboratory characterization of the structural properties controlling dynamical gas transport in Mars-analog soils. Icarus 197, 606–620.

Stephens, D.B., 1996. Vadose Zone Hydrology. CRC Lewis, Boca Raton, 347pp.

Stillman, D.E., Grimm, R.E., 2011. Dielectric signatures of adsorbed and salty liquid water at the Phoenix landing site, Mars. J. Geophys. Res. 116. http://dx.doi.org/10.1029/2011JE003838.

Stillman et al., 2013. New observations of martian southern mid-latitude Recurring Slope Lineae (RSL) imply formation by freshwater subsurface flows. Icarus (submitted for publication).

Thoms, R.B., Johnson, R.L., Healy, R.W., 2006. User's Guide to the Variably Saturated Flow (VSF) Process for MODFLOW: U.S. Geological Survey Techniques and Methods 6-A18, 58pp.

Turcotte, D.L., Schubert, G., 1982. Geodynamics. Wiley and Sons, New York, 450pp.

van Genuchten, M.T., 1980. A closed-form equation for predicting the hydraulic conductivity of unsaturated soils. Soil Sci. Am. J. 44, 892–898.

Welty, J.R., Wicks, C.E., Wilson, R.E., 1984. Fundamentals of Momentum, Heat, and Mass Transfer, third ed. J. Wiley & Sons, New York, 803pp.

Zent, A.P. et al., 2010. Initial results from the thermal and electrical conductivity probe (TECP) on Phoenix. J. Geophys. Res. 115. http://dx.doi.org/10.1029/2009JE003420.